Hindawi
Journal of Electrical and Computer Engineering
Volume 2024, Article ID 9758163, 1 page
https://doi.org/10.1155/2024/9758163

Retraction

Retracted: Design of Image Processing Technology Support System in Human-Computer Collaborative Visual Design Assisted by Artificial Intelligence Technology

Journal of Electrical and Computer Engineering

Received 23 January 2024; Accepted 23 January 2024; Published 24 January 2024

This article has been retracted by Hindawi following an investigation undertaken by the publisher [1]. This investigation has uncovered evidence of one or more of the following indicators of systematic manipulation of the publication process:

(1) Discrepancies in scope

(2) Discrepancies in the description of the research reported

(3) Discrepancies between the availability of data and the research described

(4) Inappropriate citations

(5) Incoherent, meaningless and/or irrelevant content included in the article

(6) Manipulated or compromised peer review

The presence of these indicators undermines our confidence in the integrity of the article's content and we cannot, therefore, vouch for its reliability. Please note that this notice is intended solely to alert readers that the content of this article is unreliable. We have not investigated whether authors were aware of or involved in the systematic manipulation of the publication process.

Wiley and Hindawi regrets that the usual quality checks did not identify these issues before publication and have since put additional measures in place to safeguard research integrity.

We wish to credit our own Research Integrity and Research Publishing teams and anonymous and named external researchers and research integrity experts for contributing to this investigation.

The corresponding author, as the representative of all authors, has been given the opportunity to register their agreement or disagreement to this retraction. We have kept a record of any response received.

References

[1] Y. Song, "Design of Image Processing Technology Support System in Human-Computer Collaborative Visual Design Assisted by Artificial Intelligence Technology," *Journal of Electrical and Computer Engineering*, vol. 2023, Article ID 9363644, 15 pages, 2023.

Hindawi
Journal of Electrical and Computer Engineering
Volume 2023, Article ID 9363644, 15 pages
https://doi.org/10.1155/2023/9363644

Research Article

Design of Image Processing Technology Support System in Human-Computer Collaborative Visual Design Assisted by Artificial Intelligence Technology

Yan Song

Zhengzhou Railway Vocational & Technical College, Zhengzhou, Henan 450000, China

Correspondence should be addressed to Yan Song; 10497@zzrvtc.edu.cn

Received 31 December 2021; Revised 28 March 2022; Accepted 23 March 2023; Published 8 May 2023

Academic Editor: Muhammad Rashad

Aiming at the problems of high cleaning intensity, low efficiency, and hidden safety hazards of high-altitude curtain walls, this study proposes that the image processing method is a kind of image processing technology in human-computer collaborative visual design. The algorithm uses generalized mapping to scramble the picture and then expands and replaces the scrambled pictures one by one through the image processing technical support system. Studies have shown that this calculation method has mixed pixel values, good diffusion performance, and strong resistance performance. The pixel distribution of the processed image is relatively random, and the features of similar loudness are not relevant. It is proved through experiments that the above calculation methods have strong safety performance.

1. Introduction

With the development of science and technology and Internet technology, multimedia digital products are widely used in all walks of life. Nowadays, many security issues are gradually exposed in the dissemination and use of multimedia data information. The characteristics of digital pictures are large data and high correlation between data. In the past, traditional processing methods used for multimedia processing have the disadvantage of low efficiency [1, 2]. The development of a new type of chaotic system, which makes multimedia image processing have the characteristics of high efficiency and high safety performance, is a research boom in recent years. There are many types of image data processing in human-computer collaborative visual design. Due to the high dimensions, image processing in human-computer collaborative visual design leads to undesirable results. The multigranularity algorithm of image data in human-computer collaborative visual design proposed in literature [3] should not be applied to the fusion of high-level data clusters because image data in human-computer collaborative visual design cannot be processed to the hypotenuse boundary. In literature [4], a weighted processing algorithm for image data processing in human-computer collaborative visual design is proposed. The error in the processing result is relatively large. In the literature [5], due to the dispersiveness of the algorithm in the use process, the image data processing analysis in the human-computer collaborative visual design based on a priori information is proposed.

This study designs a robot control system with STM 32 and LPC 4300 as the control core. The control system adopts a motion control method based on electric push rods, servo motors, and vacuum suction cups and adds an image recognition control system. This paper studies the image processing method in the human-machine collaborative visual design of the high-order chaotic calculation method. The experimental analysis shows that this method has strong resistance to exhaustive supply and system analysis attacks, high computational efficiency, and high security performance.

2. Control System Design Methods

As shown in Figure 1, the man-machine image processing technology support system here mainly includes man-

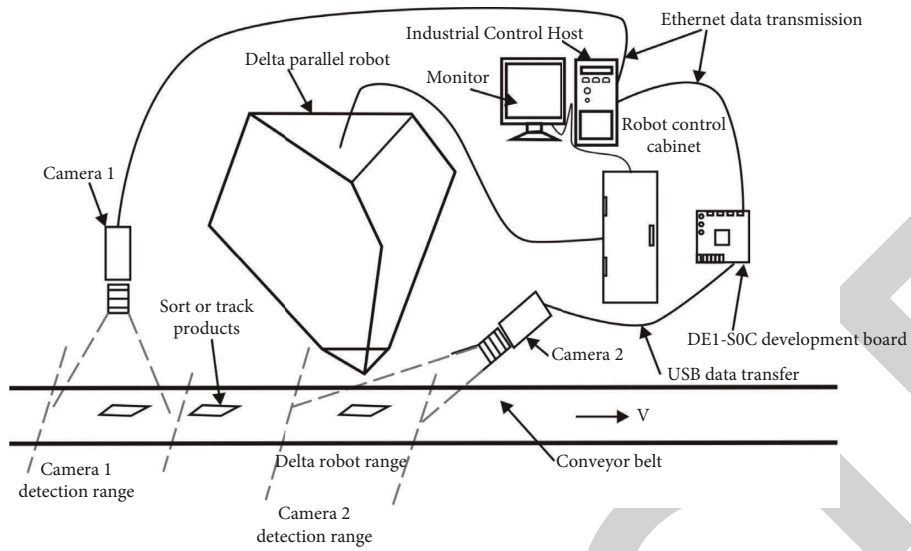

Figure 1: Human-machine image processing technology support system.

machine, transmission mechanism, and vision system. The dynamic capture experiment platform constitutes a semi-closed circulating conveying system to ensure that the capture target moves cyclically on the conveyor belt [6].

2.1. Control System Hardware Design. According to the design requirements, the hardware design of the system includes two parts: the hardware design of the main controller based on STM 32 and the hardware design of the machine vision control system based on LPC 4300 [7], and a simplified block diagram of the hardware design of the control system is shown in Figure 2.

The hardware of the man-machine image processing technology support system in this article mainly composed of light source, CCD industrial camera, camera lens, and artificial intelligence technology. The specific hardware selection is as follows.

2.1.1. Light Source. The light source has a huge impact on data collection and system performance. In the human-machine vision system, a good light source can highlight the characteristics of the captured target as much as possible. The part that needs to be detected and the part that needs to be captured can achieve a greater difference, thereby ensuring the feature difference of the target to be detected in other backgrounds. The characteristic comparison of different light sources is shown in Table 1.

Considering the actual working situation of the human-machine grasping system in the grasping process, because the brightness of the fluorescent lamp is relatively large, it is suitable for large-area uniform lighting and the price is cheap [8, 9]. Therefore, to ensure better lighting effects, this article uses fluorescent lamps as humans. The light source installation design of the vision system is shown in Figure 1.

2.1.2. CCD Industrial Camera. Choosing a suitable industrial camera is very important for the human-machine vision control system. In this study, the visual inspection area based on artificial intelligence technology is 300 mm × 200 mm, and the accuracy should be kept within 0.5 slowly. Therefore, the No. 1 industrial camera uses a 2 million pixel (1600 × 1200) camera. The No. 2 industrial camera uses a 2 million pixel (1280 × 960) camera. Because the frame rate has a great impact on the real-time feedback of the human-machine visual inspection system, the frame rate cannot be too low [4]. Based on the above analysis, the parameters of the No. 1 industrial camera and the No. 2 industrial camera are shown in Tables 2 and 3.

2.1.3. Lens Model Selection. Considering that the resolution of the lens needs to be matched with the resolution of the industrial camera, too low resolution will reduce the accuracy of visual inspection and too much pursuit of high resolution will increase additional production costs. The focal length between the No. 1 industrial camera and the No. 2 industrial camera can be solved by the lens focal length calculation formula [10].

$$f = w * \frac{D}{W}. \tag{1}$$

Among them, D represents the object distance; w represents the total length of the visual sensor; W represents the length of the actual project corresponding to the visual sensor. Then, it can be calculated from the above parameters that the focal length of the No. 1 industrial camera is $f = 8.5 * 300/200 = 12.75$ mm, and the focal length of the No. 2 industrial camera is $f = 4.8 * 300/200 = 7.2$ mm. After comprehensive consideration, the No. 1 industrial camera uses the Computar M3Z1228C-MP lens produced by Japan's CBC Company. The specific parameter configuration is shown in Table 4. The No. 2 industrial camera uses

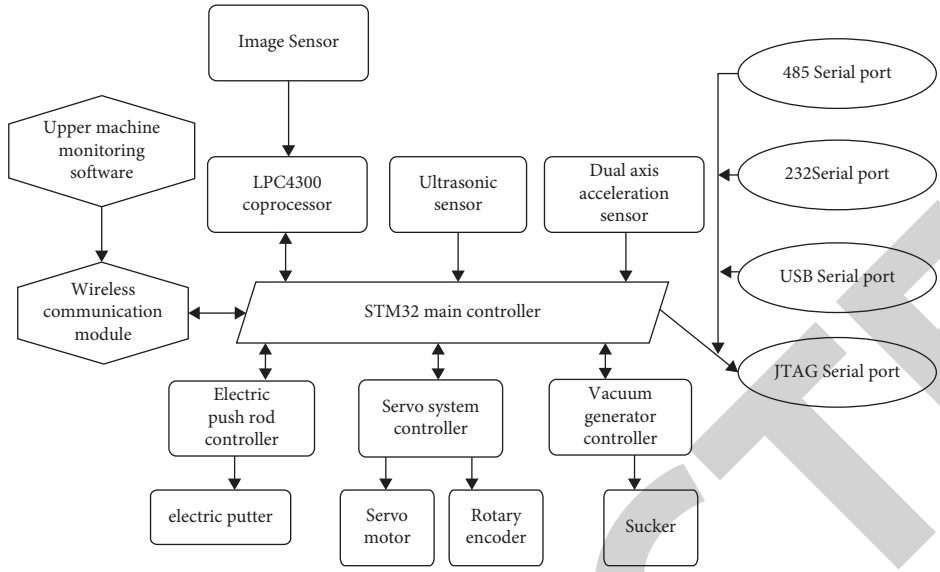

Figure 2: Simple block diagram of control system hardware design.

Table 1: Comparison of characteristics of different light sources.

Light source	Color	Life/h	Light intensity	Features
Halogen light	White, yellowish	5000–7000	Very bright	More fever, cheaper
Fluorescent lamp	White, greenish	5000–7000	Bright	Cheap, large area lighting
LED	Red, yellow, green, white, blue	60000–100000	Brighter	Cheap, small area lighting
Fiber light source	Optional	5000–7000	Bright	Less heat, uniform lighting
Electroluminescent tube	Determined by the luminous frequency	5000–7000	Brighter	Less fever, cheaper

Table 2: Parameters of industrial camera No. 1

Project	Parameter
Industrial camera model	DMK-23G74
Color	Black and white
Chip size	1/1.8 8.5 mm × 6.8 mm
Pixel	1600 × 1200
Pixel size	4.4 μm × 4.4 μm
Sensor	CCD
Frame rate	20
Interface method	C/CS interface

Table 3: Parameters of No. 2 industrial camera.

Project	Parameter
Industrial camera model	MV-UB 130GM
Color	Black and white
Chip size	1/1.3 4.8 mm × 3.6 mm
Pixel	1280 × 960
Pixel size	3.75 μm × 3.75 μm
Sensor	CMOS
Frame rate	36
Interface method	CS interface

Table 4: Lens parameters of No. 1 industrial camera.

Project	Parameter
Lens model	M3Z1228C-MP
Focal length	12.36 mm
Target surface size	2/3
Maximum imaging size	8.8 mm × 6.6 mm
Aperture range	F1.4-F16C
Working distance	0.1–∞
Interface method	C interface

Table 5: Lens parameters of No. 2 industrial camera.

Project	Parameter
Lens model	M0814-MP2
Focal length	12–36 mm
Target surface size	2/3
Maximum imaging size	8.8 mm × 6.6 mm
Aperture range	F1.4-F16C
Working distance	0.2–∞
Interface method	C interface

Computar M0814-MP2 lens. The specific parameter configuration is shown in Table 5.

The hardware design of the machine vision control system is to use the image sensor OV9715 as the image input and the LPC4300 processor as the image processing unit to realize the positioning of cleaning obstacles and the identification of cleaning objects during the cleaning process, so as to realize the intelligentization of the cleaning process. The LPC4300 is an asymmetric digital signal controller with dual core architectures of ARM3 CortexTM-M4 and Cortex-M0. It can handle a large number of data transmission and

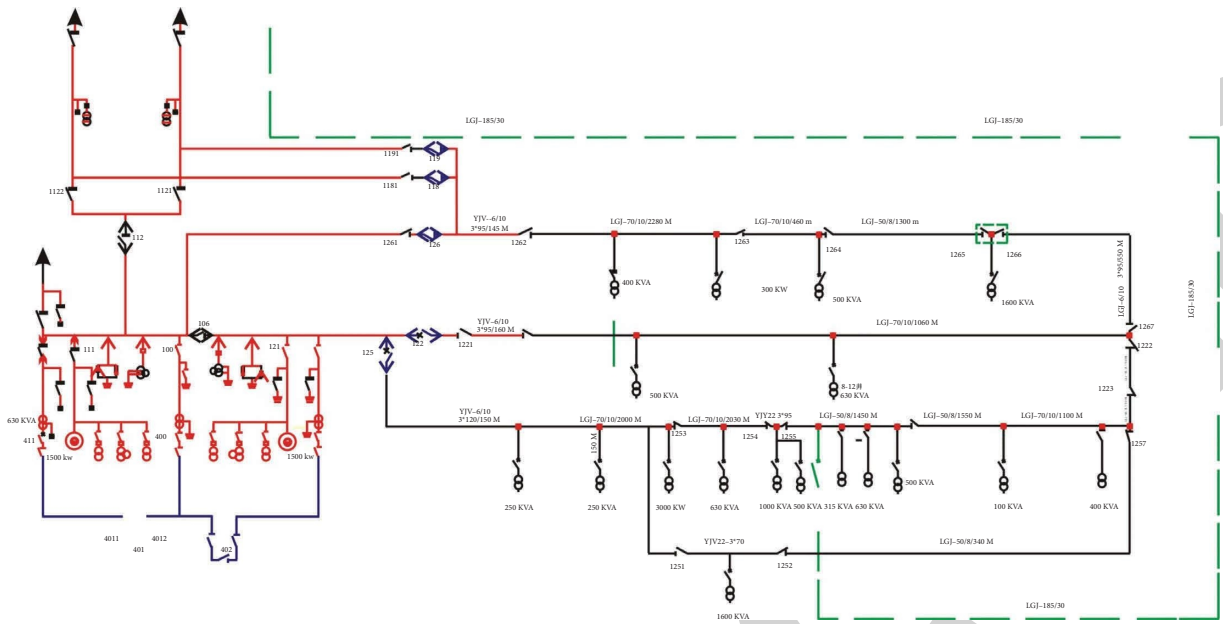

Figure 3: Hardware design of the machine vision module.

I/O processing tasks and can execute up to 204 MHz at high speed.

The OV9715 is a high-performance vision sensor with a resolution of 1 million. An ultrawide-angle lens can be used when distortion correction and image joining are required. With the first-class low-light performance of 3300 mV/(lux-sec), images can be captured under almost any lighting conditions. Figure 3 shows the hardware design of the machine vision module [11].

As shown in Figure 3, the hardware design of the image processing module includes the construction of the LPC4300 minimum system and the OV9715 drive circuit, the rudder interface and the JTAG debugging interface. The LPC4300 processor controls the steering gear to adjust the lens direction of the image processor and scans the cleaning area. The LPC4300 recognizes the image information from the image sensor and finally transmits the recognition result to STM 32. It supports communication between LPC4300 and STM 32.

2.2. Control System Software Design. Figure 4 shows the overall flow of the cleaning robot software design. The upper computer UI interface uses the wireless communication module to control the control system and set the action parameters. The control system plans the action path of the robot by collecting the data information of each sensor and the parameter information sent by the upper computer and sends the planned results to the electric push rod control system, vacuum generator control system, and servo control system. Control the washing of limbs and robotic arms.

Main controller software design: The design of the main controller application program adopts the C language program design and uses the function program library formally provided by ST Company. The functions that realize the software design of the main controller include collecting sensor data, making electric push rod, servo motor, and vacuum generator control program, and arm washing trajectory and walking trajectory plan. Figure 5 shows human-computer interaction and wireless serial. Through the demonstration, the creation of communication program and software design process of master controller are important in the design of master controller software [10].

The working system of the robot is divided into two working modes: manual working mode and intelligent working mode. In manual operation, the operator controls the robot by jog to complete the cleaning operation, which mainly realizes the monitoring and visualization of the cleaning process by the camera. Different from human work, intelligent work does not require human intervention in the robot cleaning process. The image processing module locates the cleaning obstacles and recognizes the cleaning object to automatically complete the cleaning task [11].

Image processing module software design: The software design of the image processing module is mainly the process of identifying and processing cleaning objects. During the image recognition process, the cleaning robot trains the current object in advance to obtain the feature quantity of the target object and creates an effective feature quantity mapping table. When the system is working, it extracts the characteristic value of the currently collected work object, matches it with the value of the characteristic quantity mapping table, and completes the identification of the target object. Figure 6 shows the software design flow of the image processing module.

As shown in Figure 6, the cleaning robot needs to perform preprocessing operations on the image during the image processing process. This is to simplify the image data to the greatest extent and also to improve the detectability of useful information. Image segmentation is the technique and process of segmenting an image into a number of specific

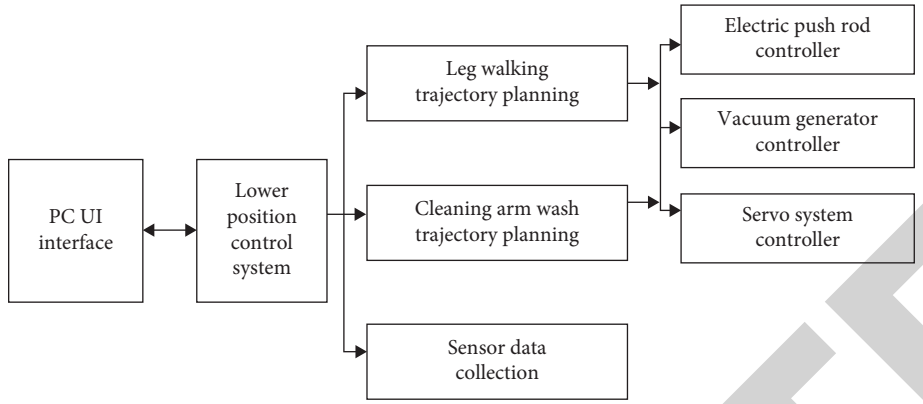

Figure 4: The overall process of system software design.

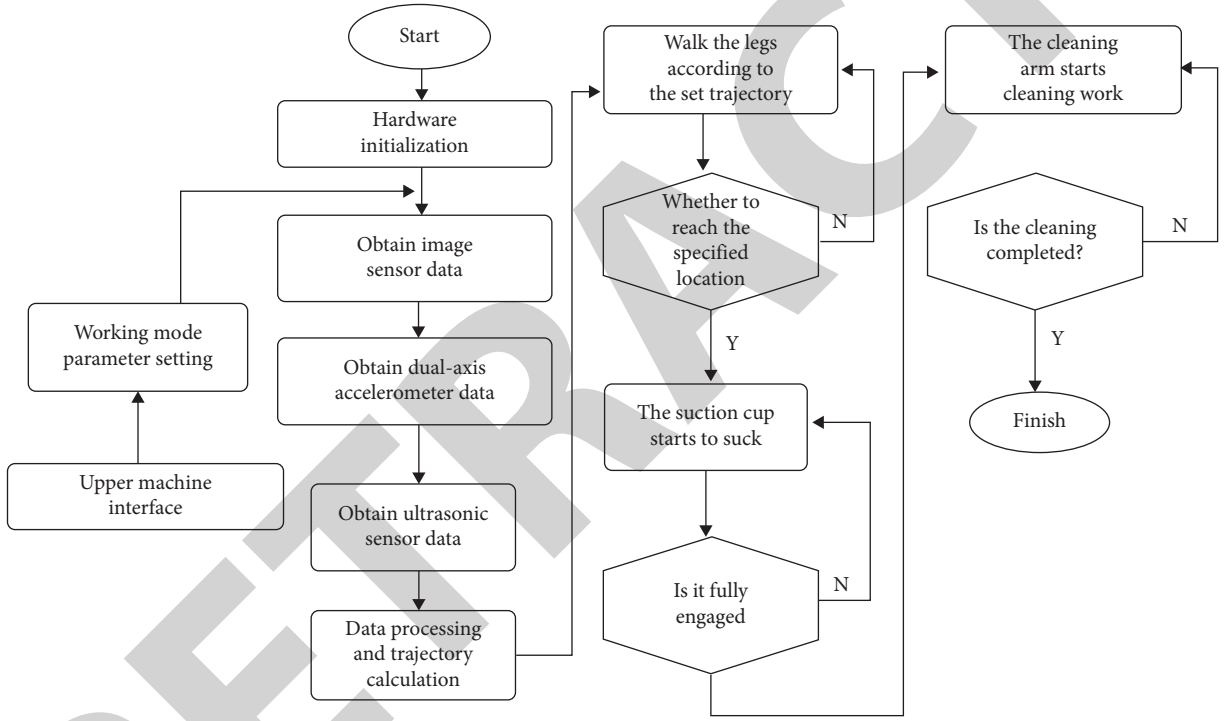

Figure 5: The main controller software design process.

areas with unique properties and proposing objects of interest. Image feature value extraction establishes a feature mapping table to match the target object to find the most effective feature from multiple features. Image matching refers to the comparison between the extracted features and the feature mapping table to achieve the purpose of target object recognition [12].

2.3. Determining the Calibration of the Positional Relationship. To enable the system to interact and track objects correctly, the positional relationship between the vision system and the conveyor belt, the robot and the conveyor belt must be calibrated. As shown in Figure 7, the coordinate system O_r-$X_rY_rZ_r$ established in the man-machine system. Suppose the business coordinate system established by the No. 1 industrial camera is O_{c1}-$X_{c1}Y_{c1}Z_{c1}$, and the field of the view coordinate system established by the conveyor plane XY in this industrial camera vision is O_{v1}-$X_{v1}Y_{v1}Z_{v1}$; the coordinate system established under the No. 2 camera is O_{c2}-$X_{c2}Y_{c2}Z_{c2}$, and the conveyor plane in this industrial camera vision. The field of the view coordinate system established by XY is O_{v2}-$X_{v2}Y_{v2}Z_{v2}$; on the conveyor belt, follow the conveyor XY plane, take the conveyor movement direction as the X axis, and use the right-hand rule to establish the world coordinate system O_w-$X_wY_wZ_w$, where O_w is the Z_{v2} axis of the O_{v2}-$X_{v2}Y_{v2}Z_{v2}$ of the coordinate system O_{v2}-$X_{v2}Y_{v2}Z_{v2}$ and the plane of the robot conveyor belt. The intersection meets the coincidence of O_w and O_{v2}. O_{v1} is the intersection point between the Z_{v1} axis of the coordinate system O_{v1}-$X_{v1}Y_{v1}Z_{v1}$ and the plane of the robot conveyor belt.

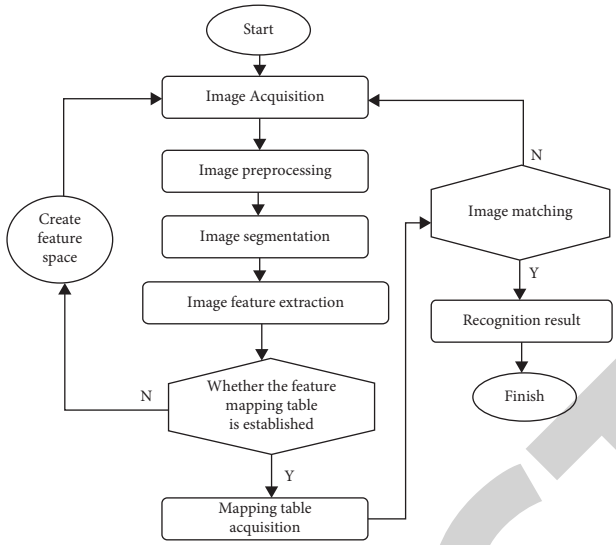

Figure 6: Image processing module software design flow.

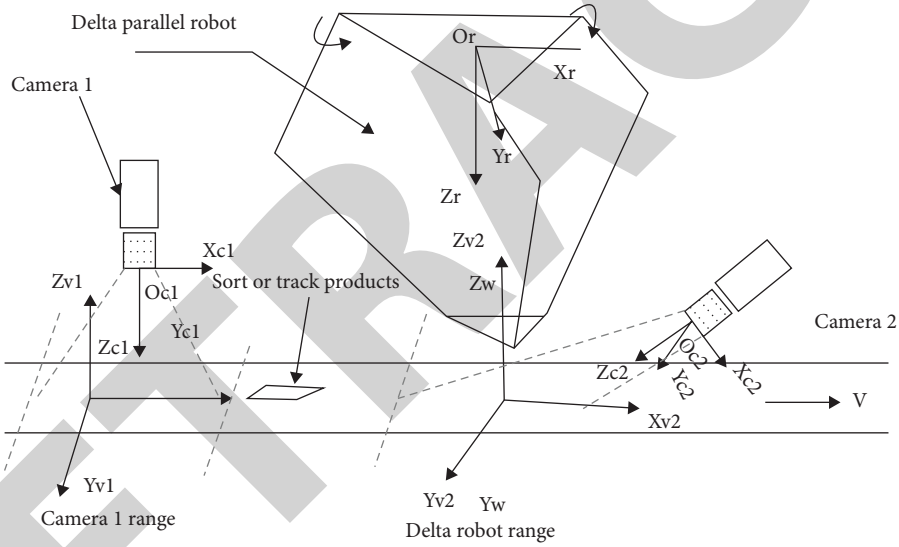

Figure 7: The relationship of the coordinate system of the man-machine control system.

It can be seen from Figure 7 that the position coordinates of a certain point $p(x_p, y_p, z_p)$ under the vision of camera No. 1 in the camera's vision area can be obtained by means of rotation and translation. If the transformation matrix from the coordinate system of camera 1 to the coordinate system of the field of view is R_{c1v1} and the translation vector is T_{c1v1}, then

$$V_{v1} = R_{c1v1}V_p + T_{c1v1}. \tag{2}$$

The industrial camera No. 1 uses point P in the coordinates, and the position coordinate formula of this point in the world coordinate system is shown in (2). Rotation coordinates are represented by R_{v1w}; translation vectors are represented by T_{v1w}.

$$V_w = R_{v1w}V_{v1} + T_{v1w}. \tag{3}$$

Similarly, for point P in the industrial camera No. 2, the position coordinates in its field of view and the rotation and translation conversion formula to the world coordinates are

$$\begin{aligned} V_{v2} &= R_{c2v2}V_p + T_{c2v2}, \\ V_w &= R_{v2w}V_{v1} + T_{v2w}. \end{aligned} \tag{4}$$

Similarly, for point P in the world coordinate system, its rotation plane formula in the machine coordinate system is as follows:

$$V_r = R_{wr}V_w + T_{wr}. \tag{5}$$

For the human-machine vision system and conveyor belt, the calibration between the robot itself and the conveyor belt is mainly based on the calculation of the abovementioned rotation matrices $R_{c1v1}, R_{c2v2}, R_{v1w}, R_{wr}$ and $T_{c1v1}, T_{c2v2}, T_{v2w}, T_{wr}$ based on the obtained data.

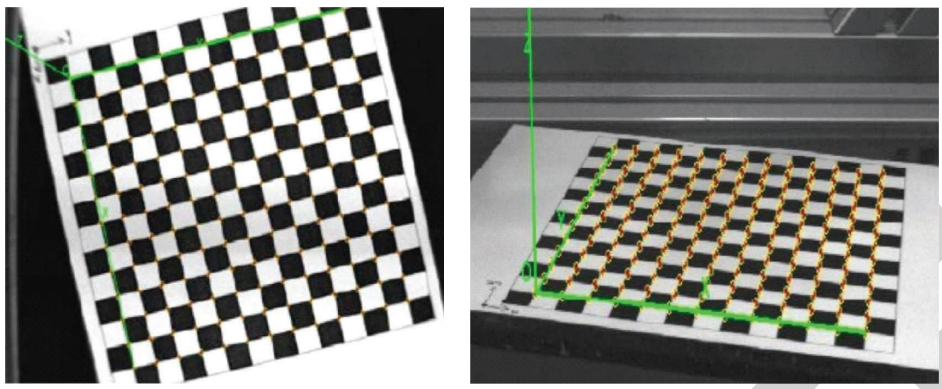

(a) (b)

Figure 8: Obtaining the calibration board coordinate system. (a) The coordinate system of the calibration plate obtained by the No. 1 camera; (b) the coordinate system of the calibration plate obtained by the No. 2 camera.

3. Calibration between the Target Images

3.1. Calibration of the Parameters between the Two Industrial Camera Coordinate Systems and the Field of View Coordinate System

3.1.1. Calculate the Plane Equation Corresponding to the Conveyor Belt in the Industrial Camera Coordinate System. As can be seen from Figure 8, place the calibration board at different positions in the field of view of the industrial camera to capture the image of the target, store the image at the same time, use the MATLAB calibration toolbox to read the saved internal parameter calibration, and then use the function of external parameter acquisition to calibrate the external parameters in each image. The acquisition of external parameter calibration is to use the coordinate system on the calibration board to obtain the coordinate system in the industrial camera through rotation and translation. Carry out plane fitting to the position coordinates of these origins and finally determine the plane equation where the calibration plate is currently located, as shown in Figure 8.

Based on the above working principles and experimental methods, the origin coordinates of the calibration coordinate system are shown in Table 6, when the grasping target collected by the industrial camera No. 1 is at 15 different positions, and the calibration board is obtained when the industrial coordinates of No. 2 are collected at 15 different positions. The coordinates of the origin under the coordinates are shown in Table 7.

By fitting the above data through MATLAB, the expressions of the field of view plane equations of the No. 1 industrial camera and the No. 2 industrial camera can be calculated:

$$\begin{aligned} 0.016802x - 0.007094y + z - 333.031718 = 0, \\ 0.009708x + 2.584124y + z - 511.581412 = 0. \end{aligned} \tag{6}$$

Table 6: The coordinates of the origin of the calibration board of the No. 1 industrial camera.

No.	X (mm)	Y (mm)	Z (mm)
1	−58.5264	−63.8011	333.5227
2	67.6947	41.3830	332.1067
3	37.7501	62.0916	332.6778
4	56.3415	48.2775	332.3378
5	−67.1456	−55.6965	333.7113
6	−44.3639	−73.2236	333.1287
7	−77.4116	−52.2072	333.8364
8	−47.7349	−74.0932	333.1775
9	41.0552	55.7552	332.6581
10	57.1042	45.3162	332.7124
11	37.0819	65.8596	332.9051
12	73.0015	59.5045	332.8345
13	−86.7054	−65.0509	333.8390
14	−86.7688	−58.1968	334.0540
15	−37.1688	−59.2738	333.4790

Table 7: The coordinates of the origin of the calibration board of the No. 2 industrial camera.

No.	X (mm)	Y (mm)	Z (mm)
1	−3.5967	16.4759	469.2558
2	−39.8526	16.4012	468.6889
3	−97.4704	16.5184	468.9079
4	92.1832	−25.9968	577.0119
5	3.7051	−25.7642	576.9291
6	−6.7059	30.0554	432.8186
7	−97.5993	30.4785	432.8319
8	−0.8004	13.3125	477.6422
9	−108.9302	13.9342	477.9089
10	−108.9306	14.8525	476.8875
11	107.6221	−14.8473	549.3964
12	18.2715	−14.4572	549.4243
13	122.1851	−28.2901	583.4863
14	13.0369	−28.2903	583.5664
15	−3.5967	−20.2878	563.0148

3.1.2. Coordinate System Establishment and Parameter Calibration. After obtaining the plane equation, assuming the intersection point $O - X_vY_vZ_v$ of the plane equation and the Z_v axis in the industrial camera coordinate system $Q(0, 0, q)^T$, $q_1 = 333.031718, q_2 = 511.581412$ can be calculated according to the expressions (3.31) and (3.32), and

then select one from the captured target image. The image of the calibration board is used as the reference image. Assuming that the external parameter corresponding to this image is (R_{vc}, T_{Vc}), R_{vc}, T_{Vc} in turn represents the rotation matrix and translation vector from the coordinate system of the calibration board to the coordinate system of the industrial camera. Select the Q point as the origin, the XY plane selects the transmission belt plane [13, 14], and construct the coordinate system $O_{v-}X_vY_vZ_v$ parallel to the X axis in the reference image, as shown in Figure 9. The $O-XYZ$ in the figure is the coordinate system of the calibration board corresponding to the reference image.

From the coordinate system of the industrial camera to the field of view coordinate system, the rotation matrix and parallel movement vector equation,

$$\begin{cases} R_{cv} = R_{vc}^{-1}, \\ T_{cv} = -R_{vc}^{-1}T_{vc}. \end{cases} \tag{7}$$

The coordinate reference image selected from the images collected by the industrial camera is Figures 10(a) and 10(b) in turn. Then, obtain the external parameters through MATLAB and obtain the formulas (8) and (9) of the conversion matrix of the industrial camera.

$$M_{v1c1} = \begin{bmatrix} R_{v1c1} & T_{v1c1} \\ 0 & 0 \end{bmatrix} = \begin{bmatrix} -0.0024 & 0.9998 & -0.0182 & 0 \\ 0.9999 & 0.0025 & 0.0082 & 0 \\ 0.0082 & -0.0182 & -0.9998 & 333.0317 \\ 0 & 0 & 0 & 1 \end{bmatrix}, \tag{8}$$

$$M_{v2c2} = \begin{bmatrix} R_{v2c2} & T_{v2c2} \\ 0 & 0 \end{bmatrix} = \begin{bmatrix} -0.9999 & -0.0126 & -0.0015 & 0 \\ -0.0061 & -0.3689 & -0.9294 & 0 \\ 0.0112 & 0.9294 & -0.3690 & 511.5814 \\ 0 & 0 & 0 & 1 \end{bmatrix}. \tag{9}$$

Then, the corresponding translation parameters from the industrial camera coordinate system to the field of view coordinate system can be derived from the expression (9), as shown in the formulas (10) and (11).

$$M_{c1v1} = \begin{bmatrix} R_{c1v1} & T_{v1c1} \\ 0 & 0 \end{bmatrix} = \begin{bmatrix} -0.0024 & 0.9999 & -0.0082 & -2.7444 \\ 0.9998 & 0.0025 & 0.0182 & 6.0739 \\ -0.0182 & -0.0082 & -0.9998 & 333.5135 \\ 0 & 0 & 0 & 1 \end{bmatrix}, \tag{10}$$

$$M_{c2v2} = \begin{bmatrix} R_{c2v2} & T_{v2c2} \\ 0 & 0 \end{bmatrix} = \begin{bmatrix} -0.9999 & 0.0061 & -0.0112 & -5.7148 \\ -0.0126 & -0.3689 & 0.9294 & -475.43949 \\ -0.0015 & -0.9294 & -0.3690 & 188.7874 \\ 0 & 0 & 0 & 1 \end{bmatrix}. \tag{11}$$

3.1.3. Parameter Calibration from the Industrial Field of View Coordinate System to the World Coordinate System. For the parameter calibration of the field of view coordinate system and the world coordinate system of the industrial camera, the conveyor belt is selected as the XY plane, and the space coordinate system is constructed according to the right-hand rule. Therefore, the coordinate system between the field of view coordinate system and the world coordinate system of the industrial camera can be regarded as the change between the two-dimensional plane coordinate system as shown in Figure 11. In the figure, $O_{v1-}X_{v1}Y_{v1}$ is the field of view coordinate system 1 corresponding to the No. 1 industrial camera; $O_{v2-}X_{v2}Y_{v2}$ is the field of view coordinate system 2 corresponding to the No. 2 industrial camera. $O_{w-}X_wY_w$ is the world coordinate system, in which O_{v2} and O_w overlap.

It can be seen from Figure 11 that assuming that O_{v1} moves vector $T_{v1w} = [a, b, 0]^T$ relative to the world coordinate system, the conversion matrix from the field of view coordinate system of the industrial camera to the

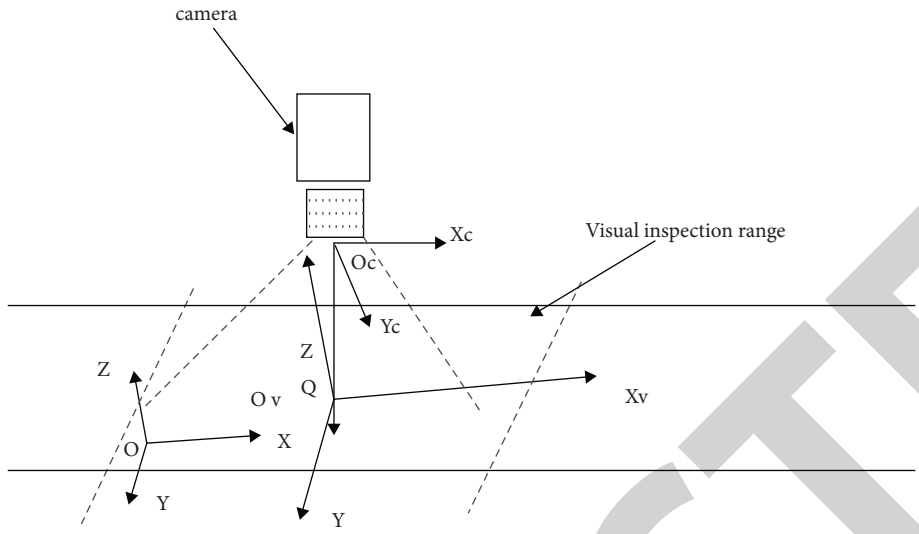

Figure 9: The relationship between the camera coordinate system and the field of view coordinate system.

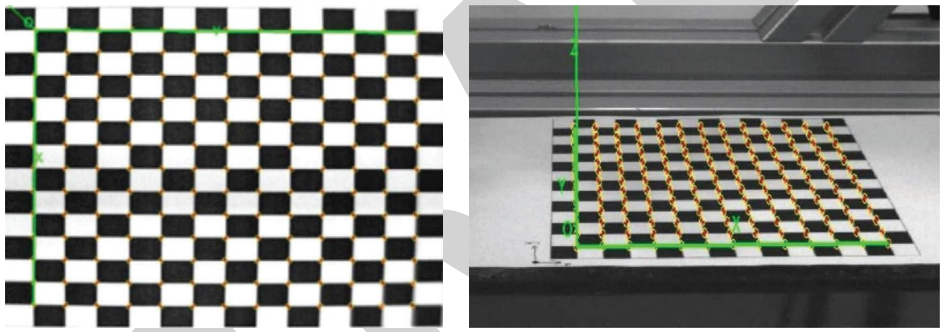

(a) (b)

Figure 10: Reference coordinate system image. (a) The reference coordinate system image of camera 1; (b) the reference coordinate system image of camera 2.

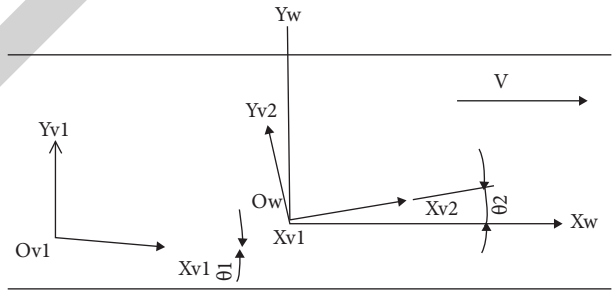

Figure 11: Conversion relationship between the field of view coordinate system of the industrial camera and the world coordinate system.

world coordinate system can be expressed by following formula:

$$M_{v1w} = \begin{bmatrix} R_{v1w} & T_{v1w} \\ 0 & 0 \end{bmatrix} = \begin{bmatrix} \cos\theta_1 & \sin\theta_1 & 0 & a \\ -\sin\theta_1 & \cos\theta_1 & 0 & b \\ 0 & 0 & 1 & 0 \\ 0 & 0 & 0 & 1 \end{bmatrix}. \quad (12)$$

Then, the matrix transformed from the field of view coordinate system 2 of the industrial camera to the world coordinate system is as follows:

$$M_{v2w} = \begin{bmatrix} R_{v2w} & T_{v2w} \\ 0 & 0 \end{bmatrix} = \begin{bmatrix} \cos\theta_2 & \sin\theta_2 & 0 & 0 \\ -\sin\theta_2 & \cos\theta_2 & 0 & 0 \\ 0 & 0 & 1 & 0 \\ 0 & 0 & 0 & 1 \end{bmatrix}. \quad (13)$$

The θ_1 and θ_2 in expressions (3.33) and (3.34) are the angles at which the field of view coordinate system of the corresponding industrial camera rotates with the Z axis as the center by the right-hand rule and then coincides with the world coordinate system. Therefore, as long as θ_1, θ_2, and T_{v1w} can be calibrated, the parameters of the corresponding transformation matrix can be obtained. The calibration process in this article is to place a positioning plate at the front of the conveyor belt and then place the target ball of the laser tracer on the positioning plate, locate as shown in Figure 12.

The image is collected by the industrial camera; use MATLAB to read the corresponding parameters in the industrial camera and then refer to the translation vector calibrated by the internal parameters; then, the industrial coordinate system corresponding to the origin of the coordinate system established by each calibration board can be obtained coordinate. Images of two calibration plates was taken by the same industrial camera at different positions; the angle formed by the line of the origin position coordinates of the corresponding calibration plates at different positions and the field of view coordinates of the industrial camera is the θ angle to be calibrated. As shown in Figure 13, the $O_{v-}X_vY_v$ and $O_{v-}X_v'Y_v'$ in the figure both transform the field of view coordinates of the industrial camera to the coordinate system of the origin of the calibration plate in the current image.

The corresponding coordinates of O_v and O_v' obtained by calibration under the coordinates of the industrial camera are V_c and V_c' in turn. Then, the formulas (12) and (13) can be transformed into the field of view coordinates. Assume that the transformed coordinates are V_v and V_c', satisfying both $V_v = (x_v, y_v, 0)^T$ and $V_v' = (x_v', y_v', 0)^T$. Then, the formula for the angle between the field of view coordinate system and the world coordinate system is as follows:

$$\theta_{vw} = \arctan\left(\frac{y_v' - y_v}{x_v' - x_v}\right). \quad (14)$$

From the results of the above calibration, combined with the transition coordinate system $O_{t-}X_tY_t$ in Figure 14, the

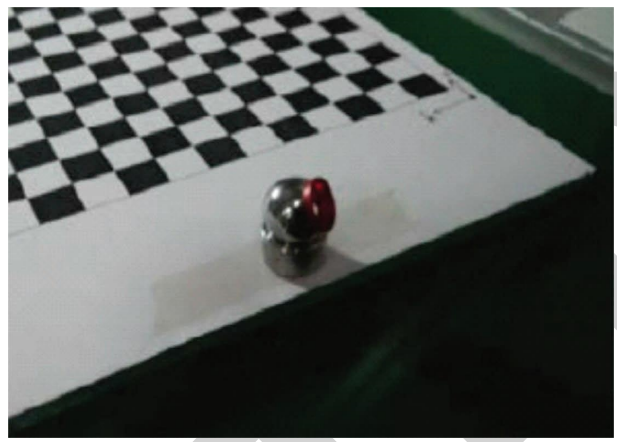

Figure 12: The placement of the target ball on the calibration plate.

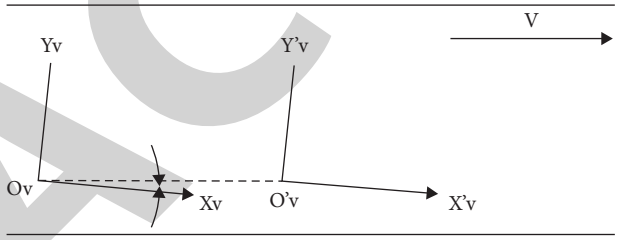

Figure 13: The rotation angle from the visual coordinate system to the world coordinate system.

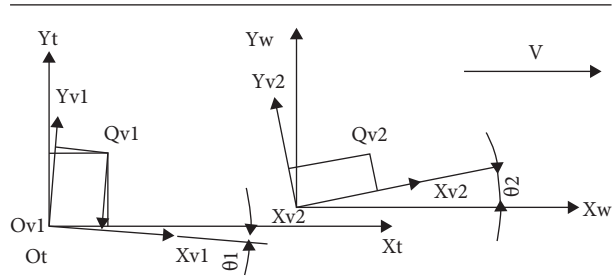

Figure 14: Schematic diagram of translation between the field of view coordinate system 1 and world coordinate system.

total length of the line segment $o_{v1}o_{v2}$ can be obtained by calculating the coordinates of the two points Q_{v1} and Q_{v2} obtained by laser tracking detection. The position coordinates of Q_{v1} and Q_{v2} corresponding to the industrial camera can be solved, and then, they can be transformed into corresponding field of view coordinates 1 and field of view coordinates 2 by formula (13) and formula (14).

According to Figure 14, Q_{v1} and Q_{v2} can be transformed into the corresponding coordinate system of $O_{t-}X_tY_t$ and $O_{w-}X_wY_w$. In addition, the position coordinate in the coordinate system is the position coordinate $Q_{v1}O_{t-}X_tY_t(x_1, y_1, 0)Q_{v2}O_{w-}X_wY_w(x_2, y_2, 0)$ in the coordinate system; then, the formula (15) of the translation

vector $T_{v1w} = (a, b, 0)^T$ can be obtained. Among them, S represents the distance measured by laser tracking.

$$T_{v1w} = \begin{bmatrix} a \\ b \\ 0 \end{bmatrix} = \begin{bmatrix} s + x_1 - x_2 \\ y_1 - y_2 \\ 0 \end{bmatrix}. \tag{15}$$

According to the above method and working mechanism, the two points corresponding to the field of view of the No. 1 and No. 2 industrial cameras on the calibration board were measured in order of 10 sets of experimental values in the industrial coordinate system, as shown in Table 8. The s value of the corresponding line segment $Q_{v1}Q_{v2}$ is shown in Tables 9 and 10.

According to formulas (13–15), the angle $\theta_1 = 3.136522$rad that the industrial camera No. 1 rotates around the Z axis and transforms to world coordinates is solved, and the angle $\theta_{12} = -0.012518$rad that the industrial camera No. 2 rotates around the Z axis and transforms to the world coordinates is solved. From formula (14) and Table 10, the translation vector $T_{v1w} = (629.942\text{mm}, -5.816852\text{mm}, 0)^T$ of the field of view coordinate system of the industrial camera No. 1 relative to the world coordinate system can be solved, and the corresponding conversion formula is as follows:

$$M_{v1w} = \begin{bmatrix} R_{v1w} & T_{v1w} \\ 0 & 1 \end{bmatrix} = \begin{bmatrix} -0.9999 & 0.0051 & 0 & 629.9424 \\ -0.0051 & -0.9999 & 0 & -5.8169 \\ 0 & 0 & 1 & 0 \\ 0 & 0 & 0 & 1 \end{bmatrix},$$

$$M_{v2w} = \begin{bmatrix} R_{v2w} & T_{v2w} \\ 0 & 1 \end{bmatrix} = \begin{bmatrix} -0.9999 & 0.0125 & 0 & 0 \\ 0.0125 & 0.9999 & 0 & 0 \\ 0 & 0 & 0 & 1 \\ 0 & 0 & 0 & 1 \end{bmatrix}. \tag{16}$$

4. Experiment and Result Analysis

4.1. Mean Filtering and Binarization to Obtain the Target Image. Binarization of the obtained target image is the basis for the completion of target recognition and location positioning. However, the acquisition of the target image is mainly affected by many factors such as brightness, sensor accuracy, conveyor belt movement deviation, and so on. It is necessary to perform necessary filtering processing on the target image to be acquired and then perform image binarization.

$$g(x, y) = \frac{1}{9} \sum_{i=-1}^{1} \sum_{j=-1}^{1} f(x + i, y + j). \tag{17}$$

At the same time, in this article, to avoid the problem of unclear image caused by the noise interference of the average filter processing of the target image, the pixel value of the filtered image is compared with the slot value of the original image, and the slot value of the two is compared. The gray value of the image is determined by the size of the image. Assuming that it represents a filtered target image, T represents a nonnegative gap value determined during the actual processing, as shown in equation (18). $g'(x, y)$

$$g'(x, y) = \begin{cases} g(x, y), & |f(x, y) - g(x, y)| < T, \\ f(x, y), & \text{others.} \end{cases} \tag{18}$$

When the filtered image is binarized, Figure 15 is obtained. It can be seen from the analysis of Figure 15 that the target area processed by the above method is clearly visible.

4.2. Obtain the Connected Area of the Target Image. The acquisition of the connected area of the image mainly marks the pixels of the same area uniformly so that this area can be distinguished from different areas, which helps to accurately identify the target in the area and accurately locate it. At present, there are many methods to extract the connected domain of a region. In this article, we use the extraction algorithm of the target connected domain based on route coding. This method only needs a Run Lengthrun-length list and an array, and sorts all courses according to the rules of 8 area connectivity to realize the rapid extraction of the connected areas of the target image.

To implement this Algorithm 1, you need to build a linked list pointer pRunLenth and an integer array. If there is an array of N length, in terms of run length, the data structure that can be used to describe is as follows:

Define the size of the target image $M \times N$, and M represents the width value of the target image and N represents the height value of the object image, which can be the coordinates of each scanned image. The integer variable uses pTemp to indicate the tentative route pointer, pCur to indicate the current route pointer, and pPer to indicate the previous route pointer. $(i, j)1 \le i \le N, 1 \le j \le Mk = 0$ is initialized to NULL in turn.

Complete the forward loop of the path connection table through the temporary path pointer and find the path up to the sequence number of the previous row. Next, referring to equation (19), the connection status is obtained. The equation R represents the number of the previous row, and m represents the m-th row from the right to the left of the previous row. At the time of $p\text{Temp}(i-1)$, the m-th route representing the previous row was connected to the route at that time. At that time, it indicated that the m-th route forward was inconsistent with the route at that time. con = 1con = 0.

$$\text{con}_R^m = \begin{cases} 1 \quad \text{if} \begin{cases} p\text{Cur} -> i\text{Start} < p\text{Temp} -> i\text{Start} - 1 \\ p\text{Cur} -> i\text{End} \ge p\text{Temp} -> i\text{End} - 1 \end{cases}, \\ 1 \quad \text{if} \begin{cases} p\text{Cur} -> i\text{Start} \ge p\text{Temp} -> i\text{Start} - 1 \\ p\text{Cur} -> i\text{End} \le p\text{Temp} -> i\text{End} - 1 \end{cases}, \\ 0 \quad \text{others}. \end{cases} \tag{19}$$

Table 8: The value of the origin of the calibration plate in the coordinates of the No. 1 camera.

No.	x_c (mm)	y_c (mm)	z_c (mm)	x_c' (mm)	Y_c' (mm)	z_c' (mm)
1	−86.6224	−72.6984	333.3297	−86.7652	−58.1956	333.4254
2	−36.9902	−73.2582	333.4086	−37.1864	−59.2267	333.4564
3	−64.5139	−72.3965	333.7712	−64.7162	−57.3053	333.7012
4	−64.5512	−69.4667	333.7544	−64.6978	−58.6447	333.6302
5	−56.6054	−65.0509	334.0392	−56.7688	−58.1967	334.1542
6	−62.6211	−69.7435	333.2318	−62.7652	−59.2307	333.6246
7	−40.9992	−73.3284	333.9277	−40.1864	−57.4520	334.0492
8	−47.3179	−72.4622	332.9116	−47.4912	−57.3053	332.8636
9	−64.5211	−68.4372	333.7354	−64.6978	−58.2457	333.5367
10	−57.9371	−65.1032	334.4129	−58.1033	−58.1258	334.3489

Table 9: The origin of the calibration plate is in the 2 coordinates of the camera coordinate system.

No.	x_c (mm)	y_c (mm)	z_c (mm)	x_c' (mm)	y_c' (mm)	z_c' (mm)
1	124.0278	−20.1911	562.8838	23.7506	−19.5010	562.7106
2	76.6957	−19.8503	562.5072	12.6459	−19.4482	562.7851
3	110.6445	−22.7152	569.2870	49.5486	−22.5250	568.9284
4	94.5216	−22.7004	569.2402	21.0217	−22.3834	569.2005
5	119.8074	−21.2764	565.6998	40.6902	−20.9663	565.2179
6	87.7754	−21.0871	565.2967	17.7723	−20.8018	565.5518
7	114.7105	−29.6973	568.3270	48.0342	−29.3628	585.6951
8	85.5459	−29.4951	585.7893	14.1057	−29.2997	586.911
9	105.5589	−11.8971	541.4459	58.0852	−11.5703	541.2335
10	81.7106	−11.6781	541.1936	32.2806	−11.4452	541.4320

Table 10: Origin coordinate and its relative length.

No.	x_c (mm)	y_c (mm)	z_c (mm)	x_c' (mm)	y_c' (mm)	z_c' (mm)	S (mm)
1	−64.702	−62.968	333.487	67.101	−21.201	566.557	624.335
2	−58.063	−61.921	333.323	97.346	−18.863	599.971	593.062
3	−64.572	−57.837	333.538	88.254	−21.287	566.146	598.066
4	−51.712	−62.173	333.094	73.749	−19.013	599.997	617.473
5	−54.201	60.151	333.367	100.782	−19.981	562.242	596.688
6	49.874	60.151	332.571	−102.48	19.102	463.207	669.958
7	54.670	63.243	332.627	−15.624	20.667	458.327	580.132
8	50.103	60.801	332.587	−27.323	19.001	462.746	595.687
9	62.186	51.134	332.424	−43.846	23.582	451.062	620.383
10	63.824	49.764	332.060	−35.155	23.930	450.078	613.355

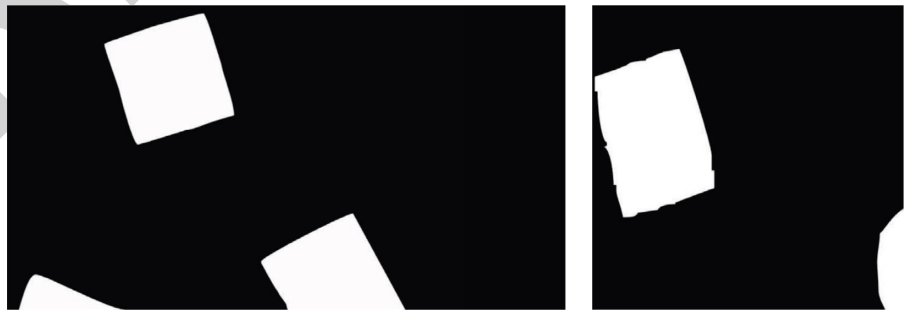

(a) (b)

Figure 15: The effect of target image binarization. (a) The image processed by the No. 1 camera; (b) the image processed by the No. 2 camera.

```
typedef struct tagRunLength
{
   int* pLable; //Pointer to the storage address of the label
   int iRow; //Current scan line number
   int iStart; //Run start column number
   int iEnd; //End of the run number
   tagRunLength* pForward; //Pointer to the previous run
   tagRunLength* pNext; //Pointer to the next run
}RunLength;
```

Algorithm 1: Data structure.

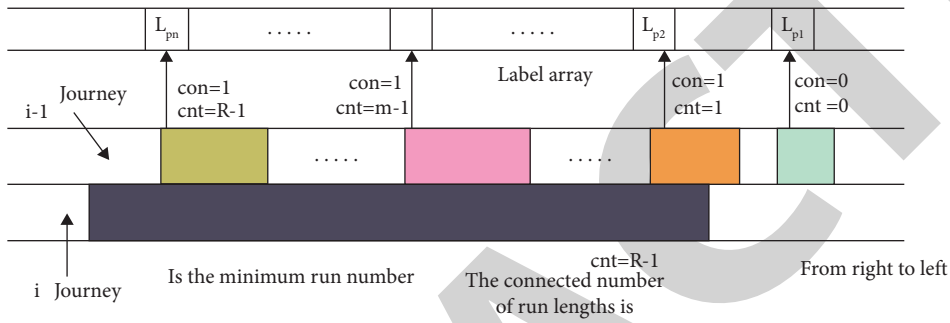

Figure 16: Connected domain processing of the target image.

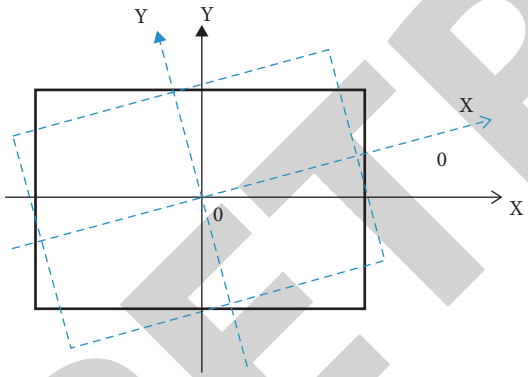

Figure 17: The angle between the smallest bounding rectangle and the regular posture.

The pCur of the current line number (i), the connected number of the pointing line can be expressed as $(i-1)$

$$\mathrm{cnt}_i = \sum_{m=0}^{R} \mathrm{con}_R^m. \tag{20}$$

For the previous line of $(i-1)$ according to the right-to-work traversal mode, refer to the expression 4.3 to judge the connectivity and calculate the run-length connectivity Cnt_i and its corresponding best sequence number $L\mathrm{min}$ according to the expression 23, as shown in Figure 16. When the number of connections of the route is satisfied, proceed to step 6. If the number of consecutive routes is satisfied, proceed to step 1.

Through the processing of the target image through the above steps, different connected domains in the image are, respectively, labeled differently.

4.3. Operation of the Smallest External Rectangle in the Connected Domain of the Image. The smallest bounding rectangle in the connected domain can not only be used to derive the rectangular degree of the target but also can be used to solve the target's position and posture θ (position and posture refers to the angle between the smallest bounding rectangle and the smallest outer rectangle of a specific posture value) as shown in Figure 17. Among them, the black solid line in the figure represents a regular posture, and the blue dashed line represents the minimum bounding rectangle of the target. This study adopts the method of constructing the rotation under the coordinates based on the center of the connected area of the image in the extraction of the smallest rectangle (Figure 17).

Assume that Si represents the minimum circumscribed rectangle of a specific posture in the established coordinate system $O - X_i Y_j$ and θi represents the rotation angle of the current coordinate relative to the coordinate system $O - X_i Y_j$. Then, the extraction process of the smallest bounding rectangle is as follows:

(1) In the initial stage, construct the coordinate system shown in Figure 18 based on the center of the target and calculate the minimum circumscribed rectangle and the corresponding area of the rectangle shown in Figure 18 that are parallel to the X axis and Y axis

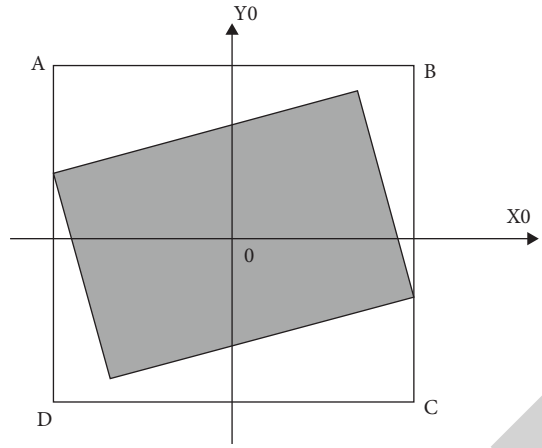

Figure 18: The circumscribed rectangle of the connected domain.

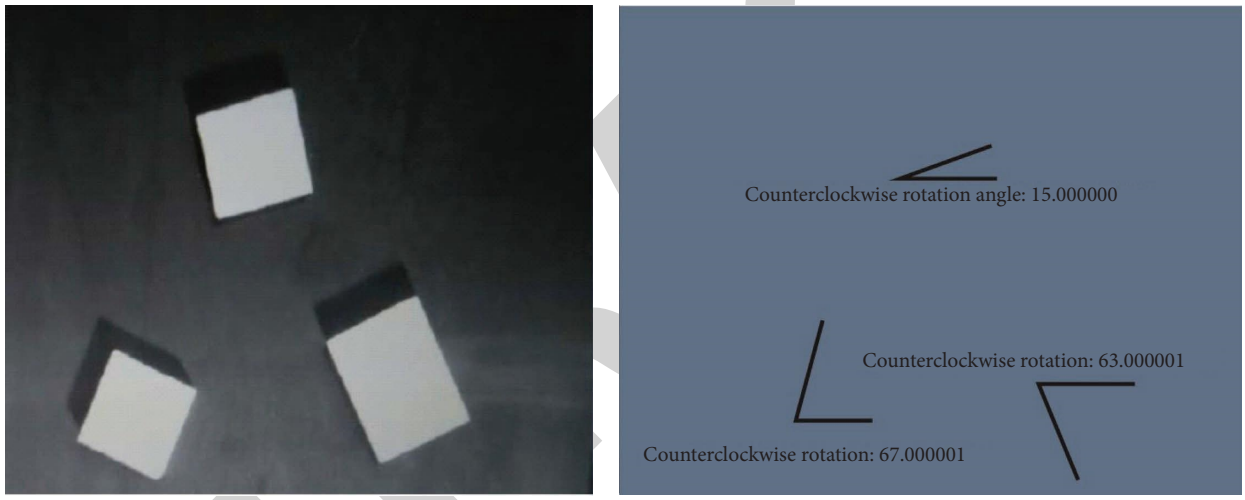

(a) (b)

Figure 19: Rotation angle detection of the target. (a) Target object on the conveyor belt; (b) detected rotation angle.

(2) Compared with the previous rotating coordinate system, the current rotating coordinate system has increased by an angle $\Delta\theta$. At the same time, calculate the corresponding minimum bounding rectangle and its area $S1$ after the rotation, and then, compare with the previous minimum area and mark the smallest of the two as $S_{\min}$. Also, the current rotation angle of $S_{\min}$ in the $O - X_i Y_j$ coordinate system is recorded as θi.

(3) Repeat step (2), always when the accumulated angle rotation exceeds the $180^\circ - \Delta = \Delta\theta$ result minus 900 to obtain the rotation angle of the corresponding regular posture, as shown in Figure 19.

5. Conclusions

As a new image processing and analysis algorithm that has gradually emerged in recent years, artificial intelligence technology can be used for the processing and analysis of image data processing in human-computer collaborative visual design. The data use different algorithms or perform multiple processing operations on the image under different conditions, and the operation results obtained by the processing operations are selected by appropriate methods to optimize the data processing and obtain the best results. This study introduces the image processing technology support system in the human-machine collaborative vision design and completes the hardware design and software design of the system's various functional modules. The experimental results show that the robot has image collection and recognition functions, which improves the robot's intelligence level.

Data Availability

The data used to support the findings of this study are available from the corresponding author upon request.

Conflicts of Interest

The author declares that there are no conflicts of interest.

References

[1] G. S. Peifeng, Y. J. Guo, X. Chen, Y. Hetong, and Z. Rongbiao, "Automatic wheat leaf rust detection and grading diagnosis via embedded image processing system," *Procedia Computer Science*, vol. 25, no. 6, pp. 2096–2102, 2017.

[2] Z. Xu, X. Shi, H. Ye, and S. Hua, "Geometric positioning and color recognition of greenhouse electric work robot based on visual processing," *International Journal of Pattern Recognition and Artificial Intelligence*, vol. 35, no. 2, pp. 2159005–2159588, 2020.

[3] G. Jiang, M. Luo, and K. Bai, "Optical positioning technology of an assisted puncture robot based on binocular vision," *International Journal of Imaging Systems and Technology*, vol. 29, no. 2, pp. 180–190, 2019.

[4] T. Wang and J. Guo, "Design and implementation of robot precise grasp based on image processing," *Manufacturing Technology & Machine Tool*, vol. 24, pp. 1012–1017, 2018.

[5] J. S. Sheu and W. H. Tsai, "Implementation of a following wheel robot featuring stereoscopic vision," *Multimedia Tools and Applications*, vol. 76, no. 23, pp. 25161–25177, 2017.

[6] E. V. Horssen, J. V. Hooijdonk, D. Antunes, and W. Heemels, "Event- and deadline-driven control of a self-localizing robot with vision-induced delays," *IEEE Transactions on Industrial Electronics*, vol. 9, no. 5, pp. 54–63, 2019.

[7] K. Yamazaki, "Robot vision applications using convolution for image processing," *Journal of the Robotics Society of Japan*, vol. 35, no. 9, pp. 644–647, 2017.

[8] L. B. Marinho, P. P. Rebouças Filho, J. S. Almeida, J. Souza, A. H. Souza Junior, and V. H. C. de Albuquerque, "A novel mobile robot localization approach based on classification with rejection option using computer vision," *Computers & Electrical Engineering*, vol. 68, pp. 26–43, 2018.

[9] X. Jin and P. Peng, "Recognizing system for state of elevator door based on robot vision," *Microcontrollers & Embedded Systems*, vol. 13, no. 2, pp. 424–436, 2018.

[10] H. E. Jia-Heng, "Application research of vision crowling robot base on adtech ar5215 robot & avs1100 vision system," *Science & Technology Vision*, vol. 26, no. 6, pp. 2-3, 2017.

[11] E. Donmez, A. F. Kocamaz, and M. Dirik, "A vision-based real-time mobile robot controller design based on Gaussian function for indoor environment," *Arabian Journal for Science and Engineering*, vol. 43, no. 12, pp. 7127–7142, 2018.

[12] L. Tingting, L. Hai, L. Youfu, Z. Zhaoli, and L. Sannyuya, "Efficient blind signal reconstruction with wavelet transforms regularization for educational robot infrared vision sensing," *IEEE*, vol. 28, no. 5, pp. 2–9, 2018.

[13] B. P. Zhu, W. Chen, H. Jian, B. Zhang, and Y. F. Xie, "Research on wall-climbing and monitoring robot of ship based on binocular vision," *Ship Science and Technology*, vol. 58, no. 4, pp. 1538–1543, 2018.

[14] L. I. Boping, "Industrial robot vision positioning technology and application," *Modern Information Technology*, vol. 39, no. 2, pp. 83–96, 2018.